Pressure-induced isostructural clustering and semiconductor-to-semimetal transition in $2H$-W(Se$_{1-x}$Te$_x$)$_2$ solid solutions: A first-principles investigation

A. Ektarawong [*]

Extreme Condition Physics Research Laboratory, Physics of Energy Materials Research Unit, Department of Physics,
Faculty of Science, Chulalongkorn University, Bangkok, 10330, Thailand
and Thailand Center of Excellence in Physics, Ministry of Higher Education, Science, Research and Innovation,
328 Si Ayutthaya Road, Bangkok 10400, Thailand

The mixing thermodynamics of Se and Te atoms in $2H$-W(Se$_{1-x}$Te$_x$)$_2$ solid solutions as well as their electronic properties under high pressure up to 45 GPa is studied using first-principles methods. The results suggest that, regardless of pressure, $2H$-W(Se$_{1-x}$Te$_x$)$_2$ exhibits a tendency toward local phase segregation into $2H$-WSe$_2$ and $2H$-WTe$_2$ (or $1T_d$-WTe$_2$) as the temperature approaches 0 K. The critical temperature, at which $2H$-W(Se$_{1-x}$Te$_x$)$_2$ is stable as a single-phase random solid solution over the entire composition range is, on the other hand, predicted to increase with the applied pressure. Upon increasing the pressure, the electronic band gap of $2H$-W(Se$_{1-x}$Te$_x$)$_2$ shrinks, and it finally undergoes the semiconductor-to-semimetal transition. The magnitude and the shrinkage rate of the band gap are found to be affected both by the degree of compression and by the alloy composition. These findings offer a possibility to engineer the electronic properties of $2H$-W(Se$_{1-x}$Te$_x$)$_2$ by varying its composition and also the pressure applied on it for future utilization of the alloy in electronic devices operating in a high-pressure environment.

I. INTRODUCTION

Heavy element-based transition metal dichalcogenides, in particular WSe$_2$ and WTe$_2$, have recently been highly of interest as promising candidates for fabricating future electronic and optoelectronic devices [1–4]. This is due mainly to their prominent intrinsic properties, including the robustness of spin-orbit coupling (SOC) [1,2,5,6]. However, for optimal utilization in relevant technological applications, materials with tunable electronic band gap, charged carrier concentration and mobility, are desirable. Practically, this can be accomplished by alloying WTe$_2$ with WSe$_2$ [7–9], as the two compounds exhibit different crystal structures and electronic characters at ambient conditions. Structurally, WSe$_2$ and WTe$_2$ are both layered materials, whose crystal structures can, in general, be described by vertically stacked layers of X-W-X (X = Se, Te) by which the interlayer interactions are dominated by the weak van der Waals forces [1,2]. At ambient conditions, WSe$_2$ crystallizes in the hexagonal $2H$ phase and behaves as a semiconductor, while WTe$_2$ that crystallizes in the orthorhombic $1T_d$ phase is semimetallic. Therefore, for a given phase of W(Se$_{1-x}$Te$_x$)$_2$, the alloying process can provide a path for engineering the materials' electronic properties by controlling its alloy composition. Recent studies [10–12] revealed WSe$_2$ undergoes isostructural semiconductor-to-semimetal transition, as it is compressed under pressure of approximately higher than 30 GPa. For this reason, pressure can, apart from composition, be considered as another variable to tailor electronic properties of W(Se$_{1-x}$Te$_x$)$_2$. It is worth noting also that, upon applying pressure above 10 GPa, WTe$_2$ has been predicted to undergo a phase transition to semiconducting $2H$ phase, which is thermodynamically stable up to about 60 GPa [13–15]. This information suggests that only the semiconducting 2H phase of W(Se$_{1-x}$Te$_x$)$_2$ should exist within the pressure range of 10–60 GPa under thermodynamic equilibrium conditions. Even though the alloying behavior of W(Se$_{1-x}$Te$_x$)$_2$ at atmospheric pressure was experimentally examined and reported in the literature [7–9], the thermodynamics of mixing of Se and Te atoms in W(Se$_{1-x}$Te$_x$)$_2$ under high pressure, and also the effect of pressure on the electronic properties of W(Se$_{1-x}$Te$_x$)$_2$ have barely been investigated. This gives rise to interesting but unanswered questions, concerning phase stability and electronic behavior of W(Se$_{1-x}$Te$_x$)$_2$ at such extreme conditions. This work thus aims to address the above questions related to $2H$-W(Se$_{1-x}$Te$_x$)$_2$, by using a cluster-expansion method in conjunction with first-principles calculations, as described in the following sections.

II. METHODOLOGY

A. Cluster-expansion method

According to the formalism, proposed in Ref. [16], the enthalpy (H) at a given pressure of $2H$-W(Se$_{1-x}$Te$_x$)$_2$ of a given atomic configuration (σ) can be expanded into a sum over the n-site correlation function of a figure (α), denoted by $\xi_\alpha^n(\sigma)$. That is,

$$H(\sigma) = N \sum_\alpha m_\alpha^n V_\alpha^n \xi_\alpha^n(\sigma). \tag{1}$$

[*]Annop.E@chula.ac.th

The factor m_α^n stands for the multiplicity of symmetry-equivalent n-site figure α, normalized to the number of sites N within configuration σ, and V_α^n is the n-site effective cluster interaction (ECI) of figure α. The correlation function $\xi_\alpha^n(\sigma)$ is, on the other hand, mathematically expressed as

$$\xi_\alpha^n(\sigma) = \frac{1}{m_\alpha^n} \sum_{\forall f \in \alpha} \left(\prod_{i=1}^n \sigma_i \right). \qquad (2)$$

Since mixing of $2H$-WSe$_2$ and $2H$-WTe$_2$ is involved particularly with Se and Te atoms residing in the chalcogen sublattice, the metal sublattice is approximated to be fully occupied by W atoms and is excluded from the expansion procedure. As a result, the spin variable σ_i takes on a value of -1 or $+1$, if site i is occupied by Se or Te, respectively, and the sum of the product run over all symmetrically equivalent figures, i.e., $f \in \alpha$. In practice, the expression of $\xi_\alpha^n(\sigma)$ must, nevertheless, be truncated at a certain cutoff radius, and the number of figures α included in the expansion is limited to a finite value.

A pool of structural models of $2H$-W(Se$_{1-x}$Te$_x$)$_2$, where $0 \leqslant x \leqslant 1$, up to 24-atom primitive supercell is firstly generated by using the algorithm of Hart and Forcade [17], and each model exhibits a unique ordered pattern of Se and Te on the chalcogen sublattice, as characterized by $\xi_\alpha^n(\sigma)$. This thus results in a total of 43 504 unique ordered solid solutions of $2H$-W(Se$_{1-x}$Te$_x$)$_2$. In the present work, the cluster expansion of the enthalpies of ordered structures of $2H$-W(Se$_{1-x}$Te$_x$)$_2$ at $p = 15$, 30, and 45 GPa is performed by using the MIT *ab initio* phase stability (MAPS) code [18], as implemented in the alloy-theoretical automated toolkit (ATAT) [19]. By following the procedure described in Refs. [20,21], the final expansion is composed of 1 zero-site, 1 on-site, 19 two-site, and 12 three-site ECIs at all considered pressures, and they fit the enthalpies of 247 selected order structures of $2H$-W(Se$_{1-x}$Te$_x$)$_2$ included in the final expansion at $p = 15$, 30, and 45 GPa with leave-one-out cross validation scores of 2.14, 2.63, and 3.11 meV/f.u., respectively. The obtained ECIs are pressure-dependent and used to predicted H at a given pressure of the remaining 43 257 ordered structures of $2H$-W(Se$_{1-x}$Te$_x$)$_2$.

The mixing enthalpy of $2H$-W(Se$_{1-x}$Te$_x$)$_2$ of a given atomic arrangement σ, $\Delta H_{\text{mix}}(\sigma)$, with $2H$-WSe$_2$ and $2H$-WTe$_2$ contents, i.e., $x_{2H\text{-WSe}_2}$ and $x_{2H\text{-WTe}_2}$, can be calculated from

$$\Delta H_{\text{mix}}(\sigma) = H(\sigma) - x_{2H\text{-WSe}_2} H_{2H\text{-WSe}_2}$$
$$- x_{2H\text{-WTe}_2} H_{2H\text{-WTe}_2}, \qquad (3)$$

where $H_{2H\text{-WSe}_2}$ and $H_{2H\text{-WTe}_2}$ are defined as the enthalpies of $2H$-WSe$_2$ and $2H$-WTe$_2$, respectively, and

$$x_{2H\text{-WSe}_2} + x_{2H\text{-WTe}_2} = 1. \qquad (4)$$

B. First-principles calculations

The first-principles enthalpies for $2H$-W(Se$_{1-x}$Te$_x$)$_2$, which are the input for the cluster expansion, at a given pressure are derived from the density functional theory by employing the projector augmented wave method [22] and the generalized gradient approximation (GGA) [23], as executed *via* the Vienna *ab initio* simulation package (VASP) [24,25]. Herein, the energy cutoff of 500 eV and the Monkhorst-Pack scheme [26] for the Brillouin-zone integration are used. The influence of SOC is included by performing self-consistent-field cycles in the noncollinear mode [27,28]. Besides, the van der Waals interactions are interpreted by the model proposed in Ref. [29]. The calculated enthalpies are assured to be converged within an accuracy of 1 meV/atom with respect to the number of **k**-point grids and the energy cutoff. During structural relaxation at a given pressure, atomic positions, volume, and cell shape of $2H$-W(Se$_{1-x}$Te$_x$)$_2$ are fully optimized.

Instead of the GGA exchange-correlation functionals, known to underestimate the electronic band gaps of materials, a meta-GGA functional (modified Becke-Johnson or mBJ [30,31]) is used, together with the tetrahedron method for the integration of the Brillouin zone [32], to obtain a more accurate description both of the electronic density of states and of the electronic band gaps of solid solutions of $2H$-W(Se$_{1-x}$Te$_x$)$_2$.

C. Special quasirandom structure technique

Besides ordered solid solutions of $2H$-W(Se$_{1-x}$Te$_x$)$_2$, ideally random solid solutions of $2H$-W(Se$_{1-x}$Te$_x$)$_2$ and of $1T_d$-W(Se$_{1-x}$Te$_x$)$_2$ are considered. Herein, the special quasirandom structure (SQS) technique [33], as implemented in Andrei V. Ruban's SPCM program [34], is employed to generate structural models of $2H$-W(Se$_{1-x}$Te$_x$)$_2$ and of $1T_d$-W(Se$_{1-x}$Te$_x$)$_2$ random solid solutions ($x = 0.25$, 0.5, and 0.75) within $4 \times 4 \times 1$ hexagonal primitive unitcells (96 atoms) and $4 \times 2 \times 1$ orthorhombic primitive unitcells (96 atoms), respectively. Within the SQS scheme, Se and Te atoms are randomly distributed on the chalcogen sublattice in such a way that the Warren-Cowley short-range-order (SRO) parameters, as representatives of two-site correlation functions $\xi_\alpha^{n=2}(\sigma)$ between Se and Te atoms, are zero or close to zero for several short-range coordination shells. The Warren-Cowley SRO parameters for the first ten coordination shells of $2H$-W(Se$_{1-x}$Te$_x$)$_2$ and of $1T_d$-W(Se$_{1-x}$Te$_x$)$_2$ random solid solutions with $x = 0.25$, 0.5, and 0.75 are listed in Tables S1 and S2 in Ref. [35], respectively.

D. Gibbs free energy calculations

The thermodynamic stability of random solid solutions of $2H$-W(Se$_{1-x}$Te$_x$)$_2$ and of $1T_d$-W(Se$_{1-x}$Te$_x$)$_2$ with respect to their most relevant constituent compounds at a given pressure p, temperature T, and composition x is evaluated by the Gibbs free energy $G(p, T, x)$,

$$G(p, T, x) = E(V, x) + F^{\text{vib}}(T, V, x)$$
$$- T S^{\text{conf}}(T, V, x) + pV. \qquad (5)$$

$E(V, x)$ is the total energy at $T = 0$ K, as can be obtained directly from the density functional theory calculations. $F^{\text{vib}}(T, V, x)$ is the Helmholtz free energy describing the vibrational contributions arising from the lattice dynamics and in general

can be expressed by

$$F^{\text{vib}}(T, V, x) = \frac{1}{2} \sum_{\mathbf{q}, \nu} \hbar \omega(\mathbf{q}, \nu, V, x)$$

$$+ k_B T \sum_{\mathbf{q}, \nu} \ln[1 - \exp(-\hbar \omega(\mathbf{q}, \nu, V, x)/k_B T)],$$

(6)

where $\omega(\mathbf{q}, \nu, V, x)$ is the vibrational frequencies at the wave vector $\mathbf{q}$ and the band index ν. $\hbar$ and k_B are the reduced Planck constant and the Boltzmann constant, respectively. In this work, the phonon calculations are performed at the quasiharmonic level using the PHONOPY package [36,37], and in order to determine the force constants, the Parlinski-Li-Kawazoe method [38] with a displacement of 0.01 Å is applied to $4 \times 4 \times 1$ hexagonal primitive unitcells (96 atoms) of $2H$-W(Se$_{1-x}$Te$_x$)$_2$ and $4 \times 2 \times 1$ orthorhombic primitive unitcells (96 atoms) of $1T_d$-W(Se$_{1-x}$Te$_x$)$_2$, all fully relaxed at different fixed volumes, i.e., the total force exerting on each atom within each supercell is less than 10^{-6} eV/Å. To assure the convergence of $\omega(\mathbf{q}, \nu, V, x)$ and $F^{\text{vib}}(T, V, x)$, the supercell's Brillouin zone is sampled with the Monkhorst-Pack $\mathbf{k}$ grids of $21 \times 21 \times 21$.

$TS^{\text{conf}}(T, V, x)$ is a contribution arising from the configurational disorder of Se and Te on the chalcogen sublattice. In the present work, S^{conf} is derived within the mean-field approach. For this reason, S^{conf} depends only on the composition x. That is,

$$S^{\text{conf}}(x) = -2k_B[x\ln(x) + (1-x)\ln(1-x)]. \qquad (7)$$

At a given temperature and chemical composition, the term pV can be obtained by fitting the sums of the first three terms in the expression of $G(p, T, x)$ at different fixed volumes to the third-order Birch-Murnaghan equation of state (EOS) [39,40], and the pressure is calculated by

$$p = -\left[\frac{\partial[E(V, x) + F^{\text{vib}}(T, V, x) - TS^{\text{conf}}(x)]}{\partial V} \right]_T. \qquad (8)$$

Since, for a given pressure and temperature, the mixing Gibbs free energies, $\Delta G(p, T, x)$, of $2H$-W(Se$_{1-x}$Te$_x$)$_2$ and of $1T_d$-W(Se$_{1-x}$Te$_x$)$_2$ disordered solid solutions are evaluated at discrete composition grids with $x = 0$, 0.25, 0.5, 0.75, and 1, the data points are fitted using a cubic spline interpolation with $\Delta x = 0.01$.

III. RESULTS AND DISCUSSION

A. Thermodynamics stability of W(Se$_{1-x}$Te$_x$)$_2$

Within the first-principles cluster-expansion approach, the mixing enthalpies (ΔH_{mix}) of 43 504 unique ordered solid solutions of $2H$-W(Se$_{1-x}$Te$_x$)$_2$, modeled with up to 24 atoms in primitive supercells, are all positive, when being evaluated with respect to $2H$-WSe$_2$ and $2H$-WTe$_2$ at $T = 0$ K and at $p = 15$, 30, and 45 GPa. This clearly suggests a tendency of isostructural decomposition of the solid solutions into their constituent compounds without forming ordering patterns of Se and Te atoms in thermodynamic equilibrium, see FIG. S1-S3 in Ref. [35]. Then, to estimate the critical temperature, at
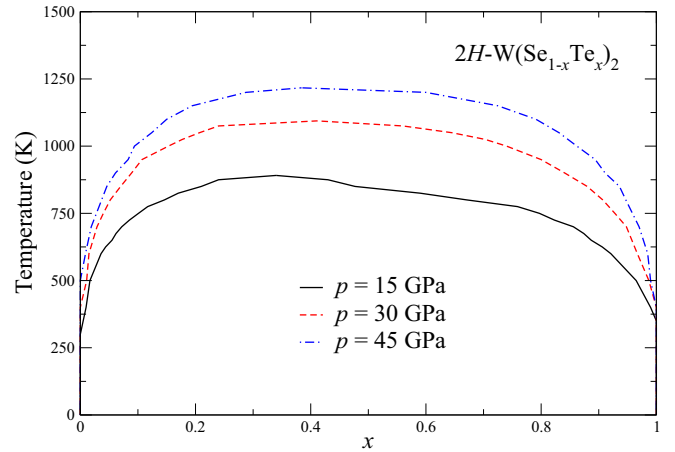

FIG. 1. Isostructural T-x phase diagram of random solutions of $2H$-W(Se$_{1-x}$Te$_x$)$_2$ at $p = 15$, 30, and 45 GPa. Here, the vibrational free energy ($\Delta F^{\text{vib}}_{\text{mix}}$) and the configurational entropy ($\Delta S^{\text{conf}}_{\text{mix}}$) arising, respectively, from the lattice vibrations and the configurational disorder of Se and Te atoms on the chalcogen sublattice are included in evaluating the mixing Gibbs free energy (ΔG_{mix}) of the random solid solutions. $\Delta F^{\text{vib}}_{\text{mix}}$ is obtained at the quasiharmonic level, while $\Delta S^{\text{conf}}_{\text{mix}}$ is estimated from the mean-field approximation.

which a continuous series of single-phase random solutions $2H$-W(Se$_{1-x}$Te$_x$)$_2$ over the whole composition range is thermodynamically stable, I determine the mixing Gibbs free energy (ΔG_{mix}) as a function of pressure, temperature, and composition of random solid solutions of $2H$-W(Se$_{1-x}$Te$_x$)$_2$, modeled by the SQS technique [33], and apply a so-called common-tangent construction to the curves of ΔG_{mix} at different fixed temperatures to outline the isostructural T-x phase diagrams of $2H$-W(Se$_{1-x}$Te$_x$)$_2$ at $p = 15$, 30, and 45 GPa, as depicted in Fig. 1. Note that, in this work, the contributions to ΔG_{mix} of $2H$-W(Se$_{1-x}$Te$_x$)$_2$ arising from the thermally induced lattice vibrations and the configurational disorder of Se and Te in the solid solutions are, respectively, obtained at the quasiharmonic level and within the mean-field approach. Figures S4, S5, and S6 display examples of ΔG_{mix} of $2H$-W(Se$_{1-x}$Te$_x$)$_2$ random solid solutions as a function of temperature and composition at $p = 15$, 30, and 45 GPa, respectively. As illustrated by Fig. 1, the critical temperature at $p = 15$ GPa is estimated to be ~900 K. That is, at $T > 900$ K, $2H$-W(Se$_{1-x}$Te$_x$)$_2$ is thermodynamically stable as a single-phase random solid solution across the entire composition range, while at $T \lesssim 900$ K there exists an immiscible region, in which $2H$-W(Se$_{1-x}$Te$_x$)$_2$ exhibits a tendency toward local segregation of $2H$-WSe$_2$ and $2H$-WTe$_2$ thus leading to a mixture of Se-rich and Te-rich $2H$-W(Se$_{1-x}$Te$_x$)$_2$ solid solutions under thermodynamic equilibrium conditions.

As can also be seen from Figs. S1–S6, ΔG_{mix} of the random solid solutions at a given temperature increase with the pressure. This subsequently leads to an increase in the critical temperature, at which the miscibility gap closes for the isostructural T-x phase diagram of pseudobinary $2H$-W(Se$_{1-x}$Te$_x$)$_2$ alloys. At $p = 30$ and 45 GPa, the critical temperature becomes ~1100 and ~1200 K, respectively. This suggests that, for a given temperature, pressure

can promote the driving force for isostructural clustering in $2H$-W(Se$_{1-x}$Te$_x$)$_2$, and thus reduce the solubility limit of Te in $2H$-WSe$_2$ and *vice versa*. By applying a so-called lever rule, one can determine, at a given pressure and temperature, the equilibrium compositions as well as the relative amount of $2H$-W(Se$_{1-x}$Te$_x$)$_2$ solid solutions in the immiscible region, as revealed in the T-x phase diagrams of pseudo-binary $2H$-W(Se$_{1-x}$Te$_x$)$_2$ alloys. In this way, the degree of segregation between Te and Se in $2H$-W(Se$_{1-x}$Te$_x$)$_2$ can be estimated. For example, at $p = 15$ GPa and $T = 750$ K, a solid solution of $2H$-W(Se$_{0.5}$Te$_{0.5}$)$_2$ will be stable as a mixture of Se-rich $2H$-W(Se$_{0.9}$Te$_{0.1}$)$_2$ and Te-rich $2H$-W(Se$_{0.2}$Te$_{0.8}$)$_2$ under thermodynamic equilibrium conditions, and the percentages of $2H$-W(Se$_{0.9}$Te$_{0.1}$)$_2$ and $2H$-W(Se$_{0.2}$Te$_{0.8}$)$_2$ presented in the $2H$-W(Se$_{0.5}$Te$_{0.5}$)$_2$ sample can approximately be 57.14% and 42.86%, respectively. The physical mechanism that promotes the chemical clustering of Se and Te atoms in $2H$-W(Se$_{1-x}$Te$_x$)$_2$ can be attributed to a considerable difference not only in atomic size, but also in electrochemical nature between Se and Te atoms. According to the Hume-Rothery rules [41], the formation of solid solutions is not to be expected, if the atomic sizes and the electronegativity of the constituent elements differ by more than 15% and 0.4, respectively. The atomic radius of Te is larger than that of Se by $\sim$22%, whereas the electronegativity between the two elements differ by 0.45. Also, the volumes of mixing of $2H$-W(Se$_{1-x}$Te$_x$)$_2$ random solid solutions, determined with respect to those of $2H$-WSe$_2$ and $2H$-WTe$_2$, are found to be positive (see Fig. S18). These analyses indicate that Se tends to interact unfavourably with Te, thus giving rise to a tendency of clustering of Se and Te atoms in $2H$-W(Se$_{1-x}$Te$_x$)$_2$. Furthermore, it is worth mentioning that, due to the use of the SQS method to model the random solid solutions and the mean-field approximation for the configurational entropy, the critical temperature of the WSe$_2$-WTe$_2$ system derived at a given pressure can generally be overestimated by 20%–30%, approximately, as compared to that obtained from the more accurate Monte Carlo simulations [42–44]. This can be attributed to the absence of the short-range ordering/clustering effect in the SQS-generated models, which is not fully compensated by the overestimation of the mean-field configurational entropy. The other source of quantitative uncertainty in the critical temperature of the system of $2H$-W(Se$_{1-x}$Te$_x$)$_2$ may be attributed to the use of the quasiharmonic approach to estimate $\Delta F_{\mathrm{mix}}^{\mathrm{vib}}$ of $2H$-W(Se$_{1-x}$Te$_x$)$_2$ random solid solutions. It has in general been accepted that at high temperatures ($\gtrsim 2/3$ of the melting temperatures of the materials under consideration at ambient pressure), $F^{\mathrm{vib}}(T, V, x)$ estimated within the quasiharmonic approximation can be less quantitatively accurate, as atoms constituting the materials strongly vibrate giving rise to anharmonicity of the lattice vibrations. Given that the melting temperatures at ambient pressure of WSe$_2$ and WTe$_2$ are $\sim$1473 and $\sim$1293 K, respectively, the quantitative uncertainty in evaluating $\Delta F_{\mathrm{mix}}^{\mathrm{vib}}$ can be expected at $T \gtrsim 900$ K. This thus gives rise also to the quantitative uncertainty in the critical temperature of $2H$-W(Se$_{1-x}$Te$_x$)$_2$, which is estimated in this work to be $\sim$900 K at $p = 15$ GPa, and increasingly so at higher pressure. However, I find that without the inclusion of the effect of lattice vibrations, the

critical temperatures of $2H$-W(Se$_{1-x}$Te$_x$)$_2$ at $p = 15$, 30, and 45 GPa are only slightly deviating from those obtained with $\Delta F_{\mathrm{mix}}^{\mathrm{vib}}$ taken into account using the quasiharmonic approach by $\sim$100 K. This indicates that the vibrational contributions are of minor importance in comparison with those arising from the configurational disorder of Se and Te atoms, and it subsequently results in the quantitative uncertainties both in the solubility limit of Te in $2H$-WSe$_2$ and vice versa at a given pressure and temperature and in the critical temperature of $2H$-W(Se$_{1-x}$Te$_x$)$_2$ at a given pressure. Such uncertainties are, nevertheless, not likely to influence the qualitative description of the results, reported in this work.

I note further that the effect of anharmonicity can in practice be more explicitly taken into consideration by implementing methods based on *ab initio* molecular dynamics simulations, for example, temperature-dependent effective potential [45,46], or those relying on the thermodynamic integration approach [47]. Implementing these sophisticated methods to investigate the anharmonicity in $2H$-W(Se$_{1-x}$Te$_x$)$_2$ is, nevertheless, beyond the scope of the present work.

It should be noted here that practical samples of WSe$_2$ in general contains two distinct phases. That is, in addition to the most common $2H$-WSe$_2$, there exists the rhombohedral 3R phase [48,49]. The two phases differ from each other only by their stacking sequence of WSe$_2$ layers along the out-of-plane axis; $2H$-WSe$_2$ exhibits a stacking sequence of AB, while 3R-WSe$_2$ has a stacking sequence of ABC. Thus it is worth exploring the possibility that, for WSe$_2$ and WTe$_2$, the 3R phases would be thermodynamically favored over the 2H phases within the pressure range of interest by calculating the enthalpies of 3R-WSe$_2$ and 3R-WTe$_2$ at different fixed pressure and comparing them with those of $2H$-WSe$_2$ and $2H$-WTe$_2$, evaluated at the same pressures. I find that, within the pressure range of 0–45 GPa, the enthalpy of 3R-WSe$_2$ is slightly higher than that of $2H$-WSe$_2$ (3–5 meV/f.u.), which is in line with what has been reported in the previous theoretical study of WSe$_2$ [50]. On the other hand, 3R-WTe$_2$ is predicted at $p = 0$ GPa to be about 20 meV/f.u. higher in enthalpy than $2H$-WTe$_2$, whereas at $p = 45$ GPa the enthalpy of 3R-WTe$_2$ becomes higher than that of $2H$-WTe$_2$ by about 120 meV/f.u. These results indicates that the 3R phases of the two constituent compounds are less stable in thermodynamic sense, as compared to their 2H phases. This also implies that the relative thermodynamic stability between the 2H and 3R phases of W(Se$_{1-x}$Te$_x$)$_2$ solid solutions at a given composition and pressure would correspondingly be similar to that of the constituent compounds, and thus the solid solutions of 3R-W(Se$_{1-x}$Te$_x$)$_2$ are not further considered in the present work. According to my calculations, the coexistence of $2H$-WSe$_2$ and 3R-WSe$_2$ in practical samples of WSe$_2$ may be attributed to the similarity between the two polytypes in terms of enthalpy.

Although WSe$_2$ and WTe$_2$ do exhibit different crystal structures at ambient conditions, a random solid solution of $2H$-W(Se$_{1-x}$Te$_x$)$_2$ can be experimentally achieved for a certain composition range [7–9]. As a complement, the thermodynamic stability of W(Se$_{1-x}$Te$_x$)$_2$ at $p = 0$ GPa is also estimated. In this case, the SQS technique is used to model random solid solutions of $2H$-W(Se$_{1-x}$Te$_x$)$_2$ and
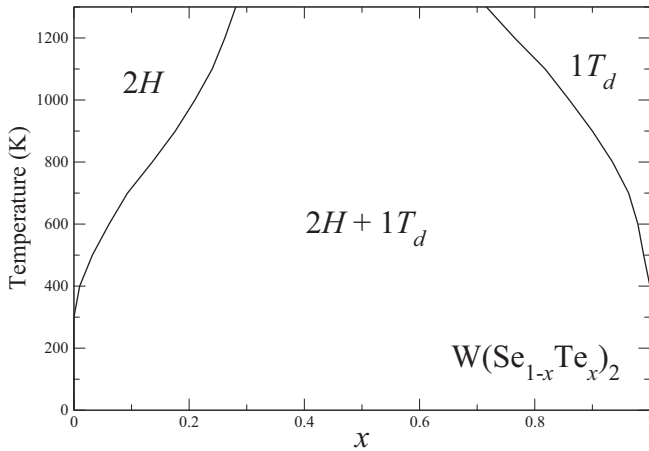
FIG. 2. T-x phase diagram of $W(Se_{1-x}Te_x)_2$, derived from the mixing Gibbs free energy (ΔG_{mix}) of $2H$-$W(Se_{1-x}Te_x)_2$ and $1T_d$-$W(Se_{1-x}Te_x)_2$ random solid solutions at $p = 0$ GPa. The vibrational free energy (ΔF_{mix}^{vib}) and the configurational entropy (ΔS_{mix}^{conf}) arising, respectively, from the lattice vibrations and the configurational disorder of Se and Te atoms on the chalcogen sublattice are included in evaluating ΔG_{mix} of the random solid solutions. ΔF_{mix}^{vib} is obtained at the quasiharmonic level, while ΔS_{mix}^{conf} is estimated from the mean-field approximation.

FIG. 3. Phonon density of states of $2H$-WSe_2, $2H$-WTe_2, and a random solid solution of $2H$-$W(Se_{1-x}Te_x)_2$ with $x = 0.5$ at $p = 0$ (black lines) and 45 GPa (red dashed lines), calculated within the harmonic approximation.

$1T_d$-$W(Se_{1-x}Te_x)_2$, and their ΔG_{mix} as a function of composition and temperature are calculated with respect to $2H$-WSe_2 and $1T_d$-WTe_2. The effects of thermally excited lattice vibrations and configurational disorder of Se and Te as well as the effect of SOC are taken into account in evaluating ΔG_{mix} of $W(Se_{1-x}Te_x)_2$ solid solutions. Figure S7 illustrates ΔG_{mix} of $2H$-$W(Se_{1-x}Te_x)_2$ and $1T_d$-$W(Se_{1-x}Te_x)_2$ at some selected temperatures. By applying the common-tangent rule to ΔG_{mix} curves both of $2H$-$W(Se_{1-x}Te_x)_2$ and of $1T_d$-$W(Se_{1-x}Te_x)_2$, the pseudo-binary T-x phase diagram of $W(Se_{1-x}Te_x)_2$ at $p = 0$ GPa is outlined, as visualized in Fig. 2. The diagram reveals the existence of a two-phase region up to very high temperature, indicating the coexistence of Se-rich $2H$-$W(Se_{1-x}Te_x)_2$ and Te-rich $1T_d$-$W(Se_{1-x}Te_x)_2$ random solid solutions, whose equilibrium compositions at a given sample composition and temperature can be obtained by using the lever rule. According to the present calculations, $\sim 25\%$ of Te (Se) can dissolve in $2H$-WSe_2 ($1T_d$-WTe_2) at $T = 1200$ K. However, according to the experimental analysis of $W(Se_{1-x}Te_x)_2$ grown at the atmospheric pressure and at $T \approx 1200$ K [9], the mixture of $2H$-$W(Se_{1-x}Te_x)_2$ and $1T_d$-$W(Se_{1-x}Te_x)_2$ exists, if $0.5 \leqslant x \leqslant 0.6$. The quantitative discrepancy in the thermodynamic stability of $W(Se_{1-x}Te_x)_2$ at such a high temperature between experiment and simulations may be attributed to (1) the effect of anharmonicity, which is not fully accessed by the quasiharmonic approximation, (2) the contributions arising from the electronic excitation, which has been neglected in the present work, and (3) the use of the SQS method, together with the mean-field approximation for the configurational entropy, to model the solid solutions of $W(Se_{1-x}Te_x)_2$. Also, since for a given pressure and temperature ΔG_{mix} of $2H$-$W(Se_{1-x}Te_x)_2$ and $1T_d$-$W(Se_{1-x}Te_x)_2$ are evaluated at discrete composition grids, as described in Sec. II D, the fitted or trending curves of ΔG_{mix} used to outline the pseudobinary T-x phase di-
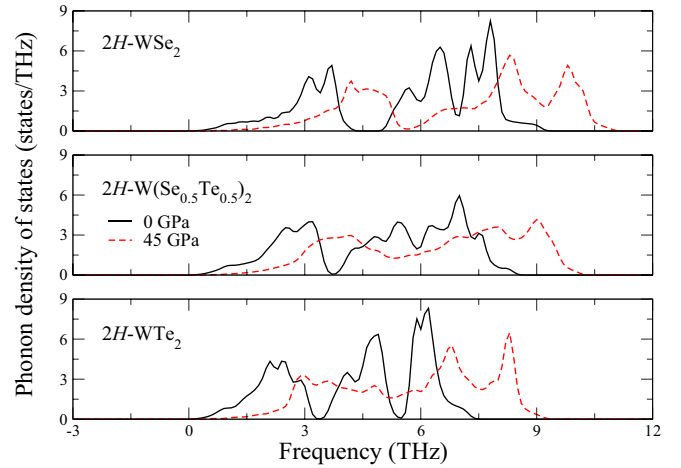
agrams of $W(Se_{1-x}Te_x)_2$ at different fixed pressure can be different depending on the choice of fitting method. This can consequently gives rise to uncertainties in, for example, the boundaries between the single-phase regions and the two-phase regions shown in Figs. 1 and 2, and be considered as another source of quantitative discrepancy in the thermodynamic stability of $W(Se_{1-x}Te_x)_2$. To further address the sources of such a discrepancy, more elaborate theoretical and experimental investigations are required.

B. Dynamical stability of $2H$-$W(Se_{1-x}Te_x)_2$

By investigating the phonon density of states and the corresponding dispersion relation of $2H$-$W(Se_{1-x}Te_x)_2$, derived within the harmonic approximation, at different fixed pressures ranging from 0 GPa to 45 GPa, I observe that the solid solutions of $2H$-$W(Se_{1-x}Te_x)_2$ and their constituent compounds do exhibit no imaginary vibrational phonon frequencies, indicating their dynamical stabilities. Figure 3 depicts the phonon density of states of $2H$-$W(Se_{1-x}Te_x)_2$ with $x = 0$, 0.5, and 1, evaluated at $p = 0$ and 45 GPa, while Figs. S8– S11 display the phonon dispersion relations of the constituent compounds at $p = 0$ and 45 GPa. I note that the phonon frequencies at $p = 0$ GPa of the two constituent compounds, derived in this work, are in good agreement with those previously reported in the literature [15,52,53]. The dynamical stability of $2H$-WTe_2 at $p = 0$ GPa further suggests that $2H$-WTe_2 and Te-rich $2H$-$W(Se_{1-x}Te_x)_2$ could remain metastable at low pressure. In practice, a random solid solution of $2H$-$W(Se_{1-x}Te_x)_2$ being metastable at ambient pressure may be achieved, for example, by quenching the solid solution, initially synthesized at high temperature ($T \approx 1200$ K) and at high pressure ($p \gtrsim 10$ GPa), to room temperature, while being compressed under such high pressure. This would prevent local segregation of Se-rich $2H$-$W(Se_{1-x}Te_x)_2$ and Te-rich $1T_d$-$W(Se_{1-x}Te_x)_2$ solid solutions during the depressurizing process because of a lack of long-range atomic diffusion at such low temperature.

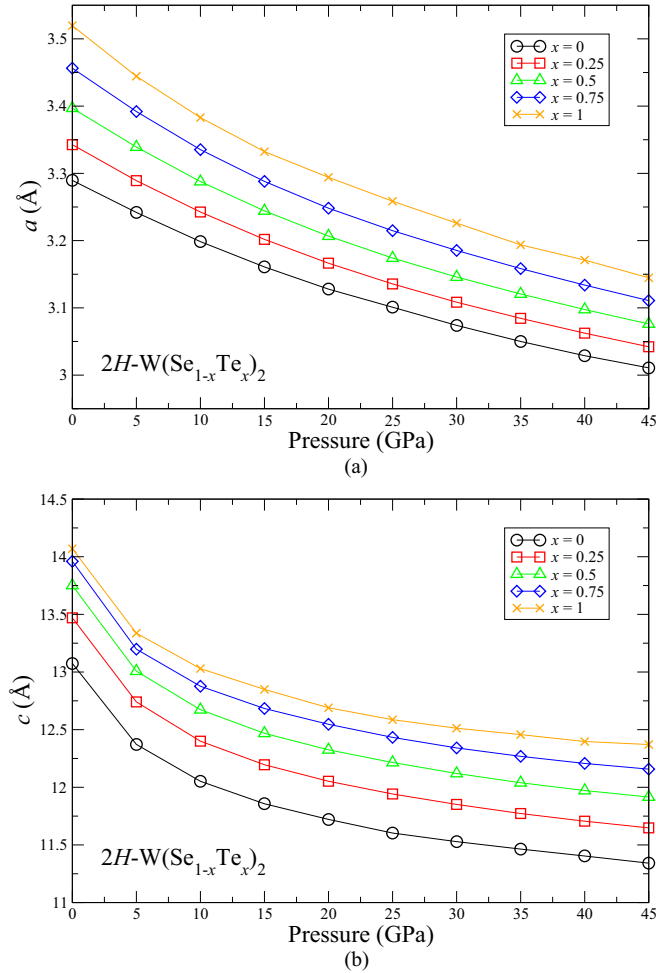FIG. 4. Pressure dependence of lattice parameters (a) a and (b) c of $2H$-W(Se$_{1-x}$Te$_x$)$_2$ random solid solutions with $x = 0$, 0.25, 0.5, 0,75, and 1, evaluated at $T = 300$ K within the quasiharmonic approximation.

FIG. 5. Unit-cell volume (V) of $2H$-WSe$_2$, as derived from the quasiharmonic approximation (black solid line), over the temperature range of 290–1000 K and at $p = 0$ GPa. Comparison is made with the experimental data (filled red circles) obtained from high-temperature x-ray diffraction method [51]. Red dashed line indicates the fitting curve drawn through the experimental data, reported in Ref. [51], by using the second order polynomial function.

C. Structural properties of $2H$-W(Se$_{1-x}$Te$_x$)$_2$

In addition to the phonon frequencies, I consider some structural properties of $2H$-W(Se$_{1-x}$Te$_x$)$_2$ random solutions and their constituents, and compare them with the available experimental data. In this work, the lattice constants a and c of $2H$-W(Se$_{1-x}$Te$_x$)$_2$ at different fixed pressures and compositions are estimated at $T = 300$ K, in which the quasiharmonic effect due to thermal expansion is taken in account (see Fig. 4 and also Figs. S12– 18). The pressure dependence of lattice parameters has to the best of my knowledge so far been measured experimentally for $2H$-WSe$_2$ only [10,11,54], while those of $2H$-W(Se$_{1-x}$Te$_x$)$_2$ where $0 < x \leqslant 1$ still awaits experimental realization. The calculated lattice parameters at $p = 0$ GPa and $T = 300$ K of $2H$-WSe$_2$ differ from the ones, derived from the x-ray diffraction technique, by less than 1.0% [54,55]. Also, the changes in lattice parameters and unit-cell volume of $2H$-WSe$_2$ with increasing applied pressure, simulated in this work, are reasonably in good agreement with the experiments [10,11,54]. Also, the volumetric thermal expansion behavior of $2H$-WSe$_2$, theoretically derived in the present work at $p = 0$ GPa, is found to

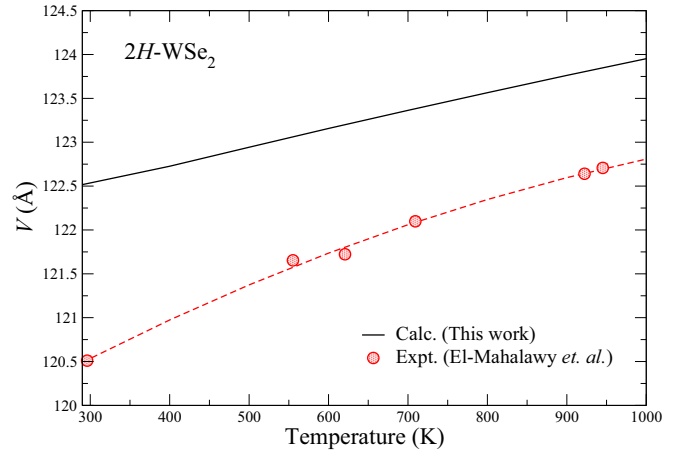be in line with that established from the experimental data measured at ambient pressure within the temperature range of 290-1000 K [51], see Fig. 5. I note that the temperature dependence of the equilibrium unitcell volume of $2H$-WSe$_2$ at $p = 0$ GPa is estimated by finding the unitcell volume of $2H$-WSe$_2$ that minimizes its Gibbs free energy $G(p, T)$, as expressed in Eq. (5), at a constant temperature. Even though the equilibrium unitcell volume as a function of temperature of $2H$-WSe$_2$ obtained from the quasiharmonic approximation is overestimated, as compared to the experimental data reported in Ref. [51], the difference in the equilibrium unitcell volume between them within such a range of temperature is tiny (less than 1.7%). These results further demonstrate the reliability of the approaches used in this work for simulating the properties of $2H$-W(Se$_{1-x}$Te$_x$)$_2$ under high pressures and high temperatures.

It can be seen that, at $p \lesssim 10$ GPa, the solid solution are more compressible along the c-axis than along the a axis. This can be attributed to the weak van der Waals interactions, coupling between the layers of X-W-X, where $X =$ Se and Te, in the solid solutions. As the applied pressure increases, the interlayer distance decreases. This results in an increase in the repulsive interactions between the adjacent layers and thus a decrease in the compressibility of the material along the c axis, until it becomes comparable to that along the a-axis at $p > 10$ GPa. The theoretical data on the pressure and composition dependence of lattice parameters for $2H$-W(Se$_{1-x}$Te$_x$)$_2$ with compositions other than $x = 0$ (Fig. 4 and FIG. S12-18) are also provided as a fingerprint for future characterization of the solid solutions. For a given pressure, the equilibrium parameters a and c of $2H$-W(Se$_{1-x}$Te$_x$)$_2$ random solid solutions show, respectively, tiny negative and distinct positive deviations from the linear Vegard's rule, which can be attributed to the difference in the lattice parameters of higher than $\sim$5% between the two constituent compounds [56].
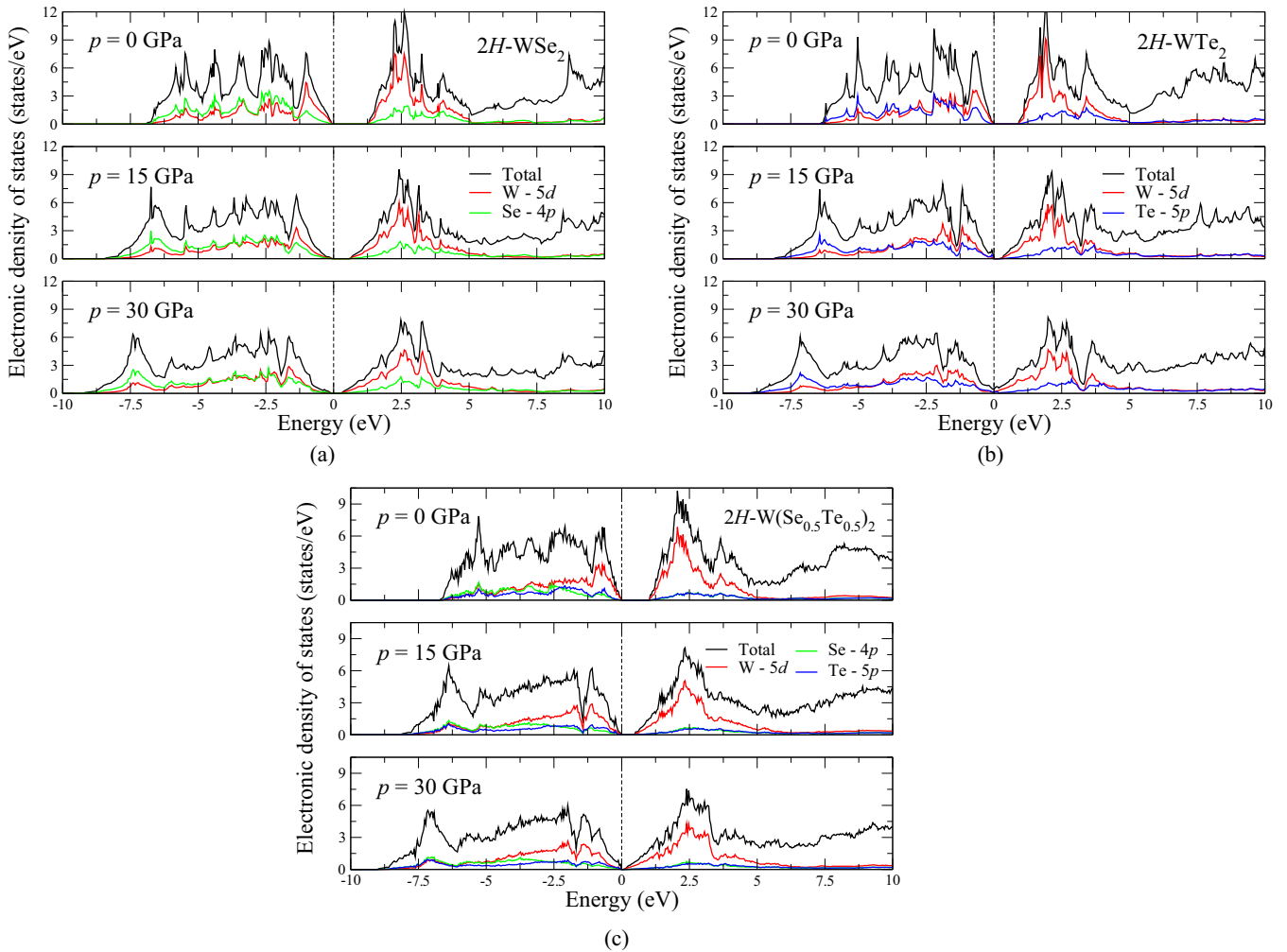
FIG. 6. Electronic density of states of (a) $2H$-WSe$_2$, (b) $2H$-WTe$_2$, and (c) $2H$-W(Se$_{0.5}$Te$_{0.5}$)$_2$ random solid solution at $p = 0$, 15, and 30 GPa, calculated with the meta-GGA functional (modified Becke-Johnson or mBJ exchange potential [30,31]). The dashed lines located at 0 eV indicate the Fermi level.

D. Electronic properties of $2H$-W(Se$_{1-x}$Te$_x$)$_2$

By investigating the mBJ-dervied electronic density of states of $2H$-W(Se$_{1-x}$Te$_x$)$_2$ solid solutions at different fixed pressures (see Fig. 6 displaying the electronic density of states of $2H$-W(Se$_{1-x}$Te$_x$)$_2$ with $x = 0$, 0.5 and 1 calculated at $p = 0$, 15, and 30 GPa), the valence and conduction bands of $2H$-W(Se$_{1-x}$Te$_x$)$_2$ are dominated by the $5d$ orbitals of W, $4p$ orbitals of Se, and $5p$ orbitals of Te. This indicates strong hybridization between these orbitals for the valence states lied just below the Fermi level, and also the covalent nature of the intralayer bonding between W and X, where $X =$ Se and Te. Upon increasing the pressure, the valence and conduction bands of $2H$-W(Se$_{1-x}$Te$_x$)$_2$ disperse, which results in reduction of their band-gap energy. Figure 7 displays the calculated values of electronic band gap of $2H$-W(Se$_{1-x}$Te$_x$)$_2$ random solid solutions at different fixed compositions and pressures. The band gaps of $2H$-WSe$_2$ and $2H$-WTe$_2$ decrease to zero at $p \approx 45$ GPa and 20 GPa, respectively, while those of the random solid solutions with $x = 0.25$, 0.5, and 0.75 decrease to zero at $p \approx 35$, 30, and 25 GPa, respectively. The closure of band gap evidences a semiconductor-to-semimetal electronic

phase transition. At $p < 20$ GPa, where $2H$-W(Se$_{1-x}$Te$_x$)$_2$ is a semiconductor over the entire composition range, the values of band gap of the solid solutions at a given pressure tend to show a negative deviation from Vegard's law. Still, it is worth emphasizing that the rate at which the band gap of $2H$-W(Se$_{1-x}$Te$_x$)$_2$ decreases upon increasing the applied pressure depends also on the composition, as can be seen from Fig. 7.

The electronic phase transition in $2H$-W(Se$_{1-x}$Te$_x$)$_2$ can be interpreted by a change of interlayer interactions from van der Waals to covalent bonding, as the solid solution is isotropically compressed under high pressure [10–12]. I note further that the results on electronic properties of the two constituent compounds carried out in this work, such as the values of electronic band gap at a given pressure and the changes of band gaps upon increasing the pressure, are qualitatively and quantitatively in line with those reported in the previous theoretical studies [12,15]. Furthermore, the band gap of $2H$-WSe$_2$ at $p = 0$ GPa calculated in this work by using the mBJ exchange potential is found to be in excellent agreement with the experimental value ($\sim$1.2 eV), measured at ambient conditions [57]. Nevertheless, it should be mentioned that, although the
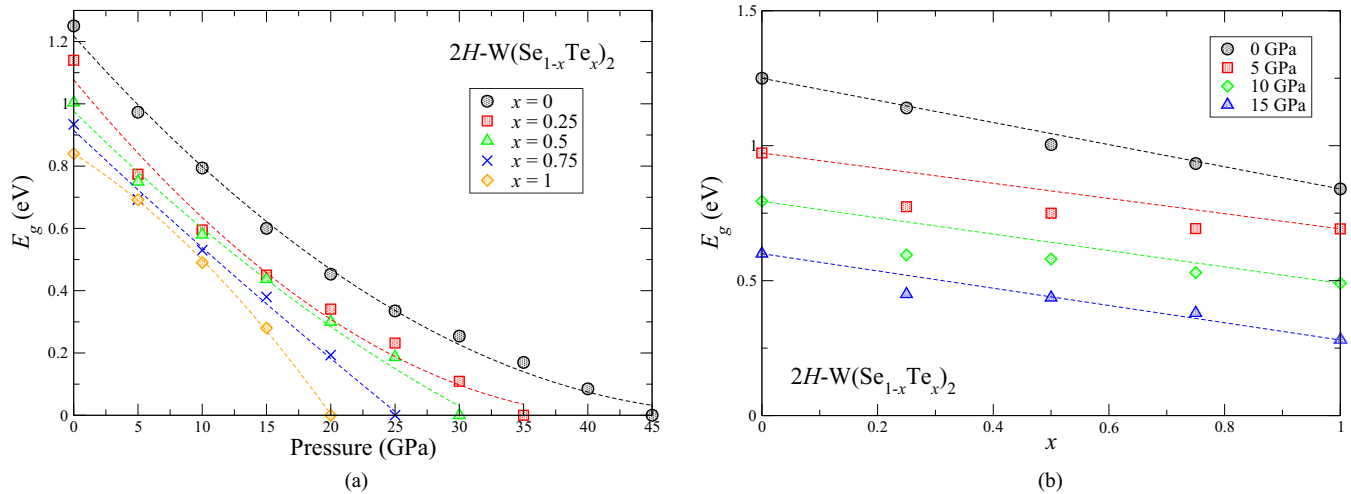
FIG. 7. [(a) and (b)] Electronic band gap (E_g) of random solid solutions of $2H$-W(Se$_{1-x}$Te$_x$)$_2$ with $x = 0, 0.25, 0.5, 0.75, 1$ at different fixed pressures ($\Delta p = 5$ GPa), derived by using the meta-GGA functional (modified Becke-Johnson or mBJ exchange potential [30,31]). The dashed lines in (a) serve only as guides to the eyes, while those in (b) indicate the linear Vegard's rule.

meta-GGA functional, i.e., mBJ, which is known to provide a better description of electronic band gap, as compared to the standard GGA exchange-correlation functionals, is used in the present work, an error in predicting the band gap as well as the electronic phase transition of $2H$-W(Se$_{1-x}$Te$_x$)$_2$ under high pressure can be expected due mainly to the approximation used for modeling the electronic exchange-correlation effects.

According to the experimental work of Shen *et al*. [10], the pressure inducing metallization in $2H$-WSe$_2$ can be as high as 51.7 GPa, which is seemingly in line with the results having been predicted in this work. On the other hand, Wang *et al*. [11] and Liu *et al*. [12] reported that the electronic phase transition in $2H$-WSe$_2$ starts at $p \gtrsim 30$ GPa, and both semiconducting phase and semimetallic phase of $2H$-WSe$_2$ coexist within the pressure range of ~ 30 to ~ 60 GPa. The coexistence of the two electronic characters of $2H$-WSe$_2$ under high pressure is probably associated either with anisotropic compression of the material or with lateral sliding of adjacent layers of WSe$_2$. This evidently points out a practical challenge to control electronic properties, especially the magnitude of band gap, of $2H$-W(Se$_{1-x}$Te$_x$)$_2$ by compressing it under high pressure.

IV. CONCLUSION

In summary, the present work reveals that, regardless of applied pressure, $2H$-W(Se$_{1-x}$Te$_x$)$_2$ exhibits chemical clustering of Se and Te atoms, as $T \rightarrow 0$ K. This results in the coexistence of Se-rich $2H$-W(Se$_{1-x}$Te$_x$)$_2$ and

Te-rich $2H$-W(Se$_{1-x}$Te$_x$)$_2$ (or Te-rich $1T_d$-W(Se$_{1-x}$Te$_x$)$_2$) solid solutions, depending on the applied pressure, under thermodynamic equilibrium conditions. The critical temperature, at which $2H$-W(Se$_{1-x}$Te$_x$)$_2$ is thermodynamically stable as a single-phase random solid solution across the whole composition range, gets higher as the pressure exerted on the material increases. For instance, the critical temperature is about 900 K at $p = 15$ GPa, while it becomes around 1200 K at $p = 45$ GPa. Upon increasing the applied pressure, the band gap of $2H$-W(Se$_{1-x}$Te$_x$)$_2$ shrinks, and eventually undergoes the semiconductor-to-semimetal electronic phase transition. In addition to the pressure, the magnitude of band gap as well as the rate at which the band gap decreases upon increasing the pressure exerted on the material depend on the composition of the solid solution. These findings offer a possibility to engineer the electronic properties of $2H$-W(Se$_{1-x}$Te$_x$)$_2$ by varying its composition and the pressure applied on it for future utilization of the solid solution in electronic devices, subjected to high-pressure compression.

[1] A. Eftekhari, Tungsten dichalcogenides (WS$_2$, WSe$_2$, and WTe$_2$): Materials chemistry and applications, J. Mater. Chem A **5**, 18299 (2017).

[2] S. Manzeli, D. Ovchinnikov, D. Pasquier, O. V. Yazyev, and A. Kis, 2D transition metal dichalcogenides, Nat. Rev. Mater. **2**, 17033 (2017).

[3] H. Zhang, Ultrathin two-dimensional nanomaterials, ACS Nano **9**, 9451 (2015).

[4] M. Chhowalla, H. S. Shin, G. Eda, L.-J. Li, K. P. Loh, and H. Zhang, The chemistry of two-dimensional layered transition metal dichalcogenide nanosheets, Nat. Chem. **5**, 263 (2013).

[5] D. Lu, A. Barinov, E. Preciado, M. Isarraraz, I. Tanabe, T. Komesu, C. Troha, L. Bartels, T. S. Rahman, and P. A. Dowben, Spin-orbit coupling in the band structure of monolayer WSe_2, J. Phys.: Condens. Matter **27**, 182201 (2015).

[6] J. Jiang, F. Tang, X. C. Pan, H. M. Liu, X. H. Niu, Y. X. Wang, D. F. Xu, H. F. Yang, B. P. Xie, F. Q. Song, P. Dudin, T. K. Kim, M. Hoesch, P. Kurmar Das, I. Vobornik, X. G. Wan, and D. L. Feng, Signature of Strong Spin-Orbit Coupling in the Large Nonsaturating Magnetoresistance Material WTe_2, Phys. Rev. Lett. **115**, 166601 (2015).

[7] A. T. Barton, R. Yue, L. A. Walsh, G. Zhou, C. Cormier, C. M. Smyth, R. Addou, L. Colombo, R. M. Wallace, and C. L. Hinkle, $WSe_{(2-x)}Te_x$ alloys grown by molecular beam epitaxy, 2D Mater. **6**, 045027 (2019).

[8] X. Qian, P. Jiang, P. Yu, X. Gu, Z. Liu, and R. Yang, Anisotropic thermal transport in van der Waals layered alloys $WSe_{2(1-x)}Te_{2x}$, Appl. Phys. Lett. **112**, 241901 (2018).

[9] P. Yu, J. Lin amd L. Sun, Q. L. Le, X. Yu, G. Gao, C.-H. Hsu, D. Wu, T.-R. Chang, Q. Zeng, F. Liu, Q. J. Wang, H.-T. Jeng, H. Lin, A. Trampert, Z. Shen, K. Suenaga, and Z. Liu, Metal-semiconductor phase-transition in $WSe_{2(1-x)}Te_{2x}$ monolayer, Adv. Mater. **29**, 1603991 (2017).

[10] P. Shen, X. Ma, Z. Guan, Q. Li, H. Zhang, R. Liu, B. Liu, X. Yang, Q. Dong, T. Cui, and B. Liu, Linear tunability of the band gap and two-dimensional (2D) to three-dimensional (3D) isostructural transition in WSe_2 under high pressure, J. Phys. Chem. C **121**, 26019 (2017).

[11] X. Wang, X. Chen, Y. Zhou, C. Park, C. An, Y. Zhou, R. Zhang, C. Gu, W. Yang, and Z. Yang, Pressure-induced iso-structural phase transition and metallization in WSe_2, Sci. Rep. **7**, 46694 (2017).

[12] B. Liu, Y. Han, C. Gao, Y. Ma, G. Peng, B. Wu, C. Liu, Y. Wang, T. Hu, X. Cui, W. Ren, Y. Li, N. Su, H. Liu, and G. Zou, Pressure induced semiconductor-semimetal transition in WSe_2, J. Phys. Chem. C **114**, 14251 (2010).

[13] C. Pu, P. Jiang, R. Yu, Y. Xu, C. Chen, and D. Zhou, Novel structural phase and superconductivity of W-Te compounds under high pressures, Comput. Mater. Sci. **188**, 110222 (2021).

[14] A. Ektarawong, P. Tsuppayakorn-aek, T. Bovornratanaraks, B. Alling, and N. Kanchanavatee, Effect of thermally excited lattice vibrations on the thermodynamic stability of tungsten ditellurides WTe_2 under high pressure: A first-principles investigation, Comput. Mater. Sci. **186**, 110024 (2021).

[15] P. Lu, J.-S. Kim, J. Yang, H. Gao, J. Wu, D. Shao, B. Li, D. Zhou, J. Sun, D. Akinwande, D. Xing, and J.-F. Lin, Origin of superconductivity in the Weyl semimetal WTe_2 under pressure, Phys. Rev. B **94**, 224512 (2016).

[16] J. M. Sanchez, F. Ducastelle, and D. Gratias, Generalized cluster description of multicomponent systems, Physica A **128**, 334 (1984).

[17] G. L. W. Hart and R. W. Forcade, Algorithm for generating derivative structures, Phys. Rev. B **77**, 224115 (2008).

[18] A. van de Walle and G. Ceder, Automating first-principles phase diagram calculations, J. Phase Equilib. **23**, 348 (2002).

[19] A. van de Walle, M. Asta, and G Ceder, The Alloy Theoretic Automated Toolkit: A User Guide, CALPHAD J. **26**, 539 (2002).

[20] A. Ektarawong and B. Alling, Stability of $SnSe_{1-x}S_x$ solid solutions revealed by first-principles cluster expansion, J. Phys.: Condens. Matter **30**, 29LT01 (2018).

[21] A. Ektarawong, B. Alling, and T. Bovornratanaraks, Role of spin-orbit coupling in the alloying behavior of multilayer $Bi_{1-x}Sb_x$ solid solutions revealed by a first-principles cluster expansion, Phys. Rev. B **101**, 134104 (2020).

[22] P. E. Blöchl, Projector augmented-wave method, Phys. Rev. B **50**, 17953 (1994).

[23] J. Perdew, K. Burke, and M. Ernzerhof, Generalized Gradient Approximation Made Simple, Phys. Rev. Lett. **77**, 3865 (1996).

[24] G. Kresse and J. Furthmüller, Efficiency of *ab-initio* total energy calculations for metals and semiconductors using a plane-wave basis set, Comput. Mater. Sci. **6**, 15 (1996).

[25] G. Kresse and J. Furthmüller, Efficient iterative schemes for *ab initio* total-energy calculations using a plane-wave basis set, Phys. Rev. B **54**, 11169 (1996).

[26] H. J. Monkhorst and J. D. Pack, Special points for Brillouin-zone integrations, Phys. Rev. B **13**, 5188 (1976).

[27] G. Kresse and O. Lebacq, VASP manual, (http://cms.mpi.univie.ac.at/vasp/).

[28] D. Hobbs, G. Kresse, and J. Hafner, Fully unconstrained noncollinear magnetism within the projector augmented-wave method, Phys. Rev. B **62**, 11556 (2000).

[29] S. Grimme, J. Antony, S. Ehrlich, and S. Kreig, A consistent and accurate *abinitio* parametrization of density functional dispersion correction (DFT-D) for the 94 elements H-Pu, J. Chem. Phys. **132**, 154104 (2010).

[30] A. D. Becke and E. R. Johnson, A simple effective potential for exchange, J. Chem. Phys. **124**, 221101 (2006).

[31] F. Tran and P. Blaha, Accurate Band Gaps of Semiconductors and Insulator with a Semilocal Exchange-Correlation Potential, Phys. Rev. Lett. **102**, 226401 (2009).

[32] P. E. Blöchl, O. Jepsen, and O. K. Andersen, Improved tetrahedron method for Brillouin-zone integrations, Phys. Rev. B **49**, 16223 (1994).

[33] A. Zunger, S.-H. Wei, L. G. Ferreira, and J. E. Bernard, Special Quasirandom Structures, Phys. Rev. Lett. **65**, 353 (1990).

[34] A. V. Ruban and I. A. Abrikosov, Configurational thermodynamics of alloys from first principles: Effective cluster interactions, Rep. Prog. Phys. **71**, 046501 (2008).

[35] See Supplemental Material at http://link.aps.org/supplemental/10.1103/PhysRevB.104.245207 for (1) supplementary figures, showing mixing enthalpy, phonon density of states, phonon dispersion relations, structural parameters, electronic band gap of $2H$-$W(Se_{1-x}Te_x)_2$ at different fixed compositions and applied pressures, (2) supplementary figures, showing mixing Gibbs free energy as a function of temperature, pressure, and composition of $2H$-$W(Se_{1-x}Te_x)_2$ and $1T_d$-$W(Se_{1-x}Te_x)_2$ random solid solutions, and (3) supplementary tables listing the Warren-Cowley short-range-order parameters for the first ten coordination shells of $2H$-$W(Se_{1-x}Te_x)_2$ and $1T_d$-$W(Se_{1-x}Te_x)_2$ random solid solutions, modeled by the special quasirandom structure method.

[36] A. Togo and I. Tanaka, First principles phonon calculations in material science, Scr Mater. **108**, 1 (2015).

[37] A. Togo, F. Oba, and I. Tanaka, First-principles calculations of the ferroelastic transition between rutile-type and $CaCl_2$-type SiO_2 at high pressures, Phys. Rev. B **78**, 134106 (2008).

[38] K. Parlinski, Z. Q. Li, and Y. Kawazoe, First-Principles Determination of the Soft Mode in Cubic ZrO_2, Phys. Rev. Lett. **78**, 4063 (1997).

[39] F. D. Murnaghan, On the theory of the tension of an elastic cylinder, Proc. Natl. Acad. Sci. USA **30**, 382 (1944).

[40] F. Birch, Finite elastic strain of cubic crystals, Phys. Rev. **71**, 809 (1947).

[41] W. Hume-Rothery, R. E. Smallman, and C. W. Harworth, *The Structure of Metals and Alloys* (Metal & Metallurgy Trust, London, 1969).

[42] B. Alling, Metal to semiconductor transition and phase stability of $Ti_{1-x}Mg_xN_y$ alloys investigated by first-principles calculations, Phys. Rev. B **89**, 085112 (2014).

[43] A. Ektarawong, S. I. Simak, L. Hultman, J. Birch, and B. Alling, First-principles study of configurational disorder in B_4C using a superatom-special quasirandom structure method, Phys. Rev. B **90**, 024204 (2014).

[44] S. Yao, W. P. Huhn, and M. Widom, Phase transitions of boron carbide: Pair interaction model of high carbon limit, Solid State Sci. **47**, 21 (2015).

[45] O. Hellman, I. A. Abrikosov, and S. I. Simak, Lattice dynamics of anharmonic solids from first principles, Phys. Rev. B **84**, 180301(R) (2011).

[46] O. Hellman, P. Steneteg, I. A. Abrikosov, and S. I. Simak, Temperature dependent effective potential method for accurate free energy calculations of solids, Phys. Rev. B **87**, 104111 (2013).

[47] A. I. Duff, T. Davey, D. Korbmacher, A. Glensk, B. Grabowski, and J. Neugebauer, Improved method of calculating *ab initio* high-temperature thermodynamic properties with application to ZrC, Phys. Rev. B **91**, 214311 (2015).

[48] W. Mortelmans, A. N. Mehta, Y. Balaji, S. El Kazzi, S. Sergeant, M. Houssa, S. De Gendt, M. Heyns, and C.

Merckling, Fundamental limitation of van der Waals homoepitaxy by stacking fault formation in WSe_2, 2D Mater. **7**, 025027 (2020).

[49] X. Wang, R. Li, H. Yang, J. Zheng, Y. Li, P. Zhu, T. Song, W. Guo, Q. Wang, J. Han, and W. Xiao, Epitaxial growth of atomically thick WSe_2 nanoribbons, Vacuum **180**, 110254 (2021).

[50] J. He, K. Hummer, and C. Franchini, Stacking effects on the electronic and optical properties of bilayer transition metal dichalcogenides MoS_2, $MoSe_2$, WS_2, and WSe_2, Phys. Rev. B **89**, 075409 (2014).

[51] S. H. El-Mahalawy and B. L. Evans, The thermal expansion of $2H - MoS_2$, $2H - MoSe_2$ and 2H-WSe_2 beween 20 and $800°C$, J. Appl. Crystallogr. **9**, 403 (1976).

[52] Y. Ding and B. Xiao, Thermal expansion tensors, Grüneisen parameters and phonon velocities of bulk MT_2 (M = W and Mo T = S and Se) from first principles calculations, RSC Adv. **5**, 18391 (2015).

[53] S. Kumar and U. Schwingenschlögl, Thermoelectric response of bulk and monolayer $MoSe_2$ and WSe_2, Chem. Mater. **27**, 1278 (2015).

[54] E. Selvi, R. Aksoy, R. Knudson, and Y. Ma, High-pressure X-ray diffraction study of tungsten diselenide, J. Phys. Chem. Solids **69**, 2311 (2008).

[55] R. Murray and B. L. Evans, The thermal expansion of $2H - MoS_2$ and 2H-WSe_2 between 10 and 320 K, J. Appl. Crystallogr. **12**, 312 (1979).

[56] K. Jacob, S. Raj, and L. Rannesh, Vegard's law: A fundamental relation or an approximation? Int. J. Mater. Res. **98**, 776 (2007).

[57] A. Prakash and J. Appenzeller, Bandgap extraction and device analysis of ionic liquid gated WSe_2 Schottky Barrier Transistors, ACS Nano **11**, 1626 (2017).